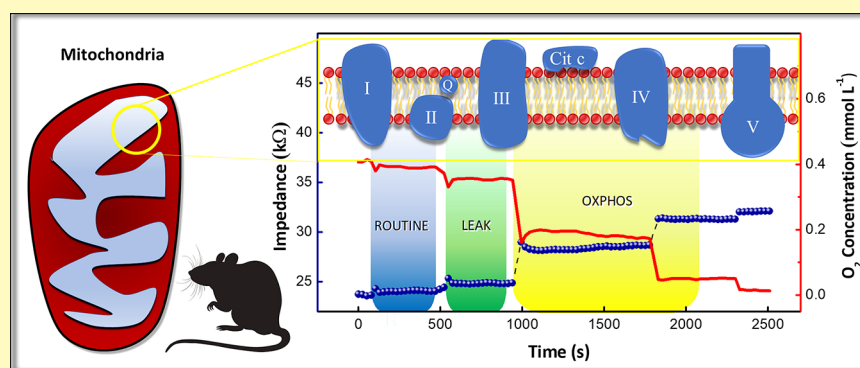# A Chemiresistor Sensor Based on Azo-Polymer and Graphene for Real-Time Monitoring of Mitochondrial Oxygen Consumption

André Olean-Oliveira,[†] Tiago Olean-Oliveira,[‡] Ana C. R. Moreno,[‡] Patrícia M. Seraphim,[‡] and Marcos F. S. Teixeira*,[†]

[†]Department of Chemistry and Biochemistry and [‡]Department of Physiotherapy, School of Science and Technology, Sao Paulo State University (UNESP), Rua Roberto Simonsen, 305, CEP 19060-900 - Presidente Prudente, São Paulo, Brazil

S *Supporting Information*

ABSTRACT: In the present study, a chemiresistor sensor based on a poly(Bismarck Brown Y)-reduced graphene oxide nanocomposite was developed to analyze the respiratory capacity of the constituent complexes of the electron transport chain. The sensorial platform was characterized using electrochemical impedance spectroscopy, and oxygen detection was accomplished by measuring the resistive properties of the sensor at fixed AC frequency. The impedance decreased significantly in response to small variations of the O_2 concentrations tested up to saturation of the electrolyte solution with molecular oxygen. The resistive response of the sensor at 0.1 Hz was linear over the oxygen concentration range from 1.17×10^{-5} mol L^{-1} to 1.02×10^{-3} mol L^{-1}, with a detection limit of 3.60×10^{-7} mol L^{-1}. Using the new O_2 sensing platform, we monitored gradients in static cultures of adherent cells exposed to graded oxygen both at rest and upon metabolic stimulation. Under high dissolved oxygen conditions, the respiration of resting cells dictated that local O_2 was moderately reduced, while cell metabolic stimulation triggered a major redistribution of O_2. The usefulness of the developed sensor was demonstrated by continuous monitoring of mitochondrial oxygen consumption in various biologic applications.

KEYWORDS: *resistive sensor, electrochemical impedance, conducting polymer, biomonitoring, mitochondrial respiratory chain activity*

Mitochondria are organelles found in eukaryotic cells, and their metabolic role is crucial for cellular functioning. The main cellular function of mitochondria is energy production (ATP), but they also act on thermogenesis, steroid synthesis, and apoptosis. The regulation of energy metabolism by mitochondria occurs through the production of ATP by the oxidation of organic substrates in the Krebs cycle, and most of the energy produced comes from the electron transport chain. This chain consists of a redox system containing five protein complexes located on the inner membrane of the mitochondria.[1] Each mitochondrial electron complex has a specific role so that, overall, the process results in the production of ATP through the consumption of molecular oxygen. Energy production is directly related to cellular oxygen concentration.[2] Mitochondrial oxygen insufficiency is indicative of structural and functional alteration of cells, tissues, and organs facing pathological conditions.[3] Furthermore, additional diseases have been investigated and found to be related to changes in the constituent complexes of the electron transport chain.[4] Currently, there are several techniques for the study and investigation of mitochondrial performance.[5] Clark-type electrodes have been utilized to monitor oxygen consumption in tissues and cells.[6]

Among the classes of electrochemical sensors, chemiresistor materials are the sensorial platform for chemical detection.[7] The response mechanism of these sensors is the change of electrical resistance based on the resonant quantum tunneling effect of the sensor material in response to a change in the chemical environment.[8] Different materials have been used as the sensorial platform in chemiresistors, such as polymers,[9] inorganic[10] and organic semiconductors,[11] and carbonaceous.[12] The combination of two or more materials can
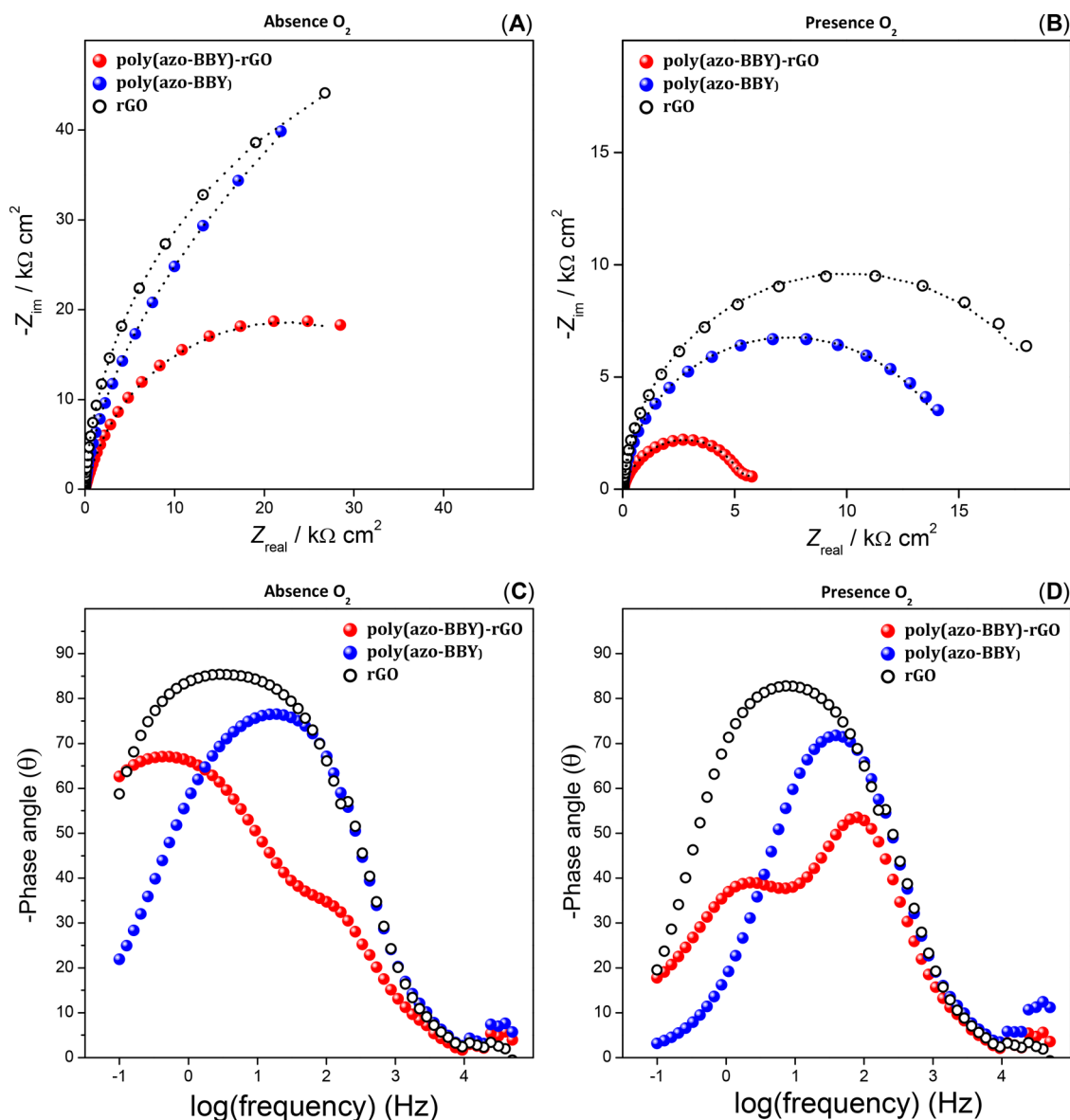
Figure 1. (A,B) Complex plane spectra for the electrode coated with poly(azo-BBY)-rGO (red circle), poly(azo-BBY) (blue circle), and rGO (open circle) in 0.05 mol L^{-1} PBS (pH 7.4) in the absence and presence of O$_2$ saturation (1.28 mmol L^{-1}), respectively. Applied potential = −0.30 V (vs SCE). Electrical equivalent circuits used for fitting the complex plane spectra are represented in Table 1. (C,D) Bode impedance diagrams for the electrode coated with poly(azo-BBY)-rGO (red circle), poly(azo-BBY) (blue circle), and rGO (open circle) in the absence and presence of O$_2$ saturation, respectively.

generate composites with new physicochemical properties taking advantage of the best properties and characteristics of each.[13] Polymer−graphene nanocomposites prepared by combining the π-conjugated system of polymers with the various properties of graphene have been highlighted.[14] In the case of azo-polymers, in addition to the advantages of being a conductive polymer, they still have the advantage of the presence of redox active sites due to the inclusion of diazonium groups in the polymer.[15]

This work presents the first report of a mitochondrial oxygen chemiresistor sensor. The sensor response was detected by measuring the electrical conductivity change of the graphene polymer by electrochemical impedance spectroscopy. Furthermore, the effects of the applied potential, applied AC frequency, and dissolved oxygen concentration on the sensor response and efficiency were examined. The use of the

proposed platform for real-time monitoring of mitochondrial oxygen in skeletal muscle cells exposed to graded oxygen both at rest and upon metabolic stimulation have been investigated in this work.

■ EXPERIMENTAL SECTION

Material and Methods. All experiments were conducted in a conventional electrochemical cell containing three electrodes: a saturated calomel electrode (SCE) as the reference electrode, a platinum wire as the counter electrode, and a fluoride-doped tin oxide (FTO) electrode coated with a poly(azo-BBY)-reduced graphene oxide (rGO) as the working electrode (1.0 cm^2). The electrodes were connected to a PalmSens3 potentiostat and managed by PSTrace 5.4 software. All reagents used were of high purity ≥98% (Sigma-Aldrich).

Preparation of the Chemiresistor Oxygen Sensor. Before coating, the FTO electrode was cleaned by immersion in an alkaline solution of 6:1:1 H$_2$O, H$_2$O$_2$ (30% v/v), and NH$_4$OH (conc.) for 5

Table 1. Parameters Determined from Fitting of the Electrochemical Impedance Spectra in Figure 1A and B, in the Absence and Presence of O_2 (1.28 mmol L^{-1}), Using Electrodes Coated with rGO, poly(azo-BBY), or poly(azo-BBY)-rGO[a]

Interface		R_{ct}	R_{ct}^*	CPE_{dl}	α_{dl}	CPE_{film}	α_{film}	Equivalent circuit
		$k\Omega\ cm^2$		$\mu F\ cm^{-2}\ s^{\alpha-1}$		$\mu F\ cm^{-2}\ s^{\alpha-1}$		
rGO/FTO	N_2	92.4	-	27.3	0.9	500	0.7	
	O_2	17.0	-	28.7	0.9	500	0.7	
pBBy/FTO	N_2	48.4	-	23.9	0.9	18.3	0.4	
	O_2	12.8	-	23.2	0.9	496	0.4	
pBBy-rGO/FTO	N_2	0.08	49.6	93.7	0.9	486	0.6	
	O_2	3.05	2.55	22.8	0.9	312	0.6	

[a]$E_{applied}$ = −0.30 V vs. SCE. R_Ω = 43 Ω cm^2. The fitting error is ≤2%.

min at 80 °C. After that, the FTO was thoroughly washed and subjected to potential cycling over the range of −0.10 to +1.40 V (vs SCE) in 0.50 mol L^{-1} H_2SO_4.

The formation of the poly(azo-BBY)-rGO nanocomposite was based on the method proposed by Teixeira et al.[15] The sensorial platform was prepared on the FTO surface by potential cycling between −0.30 and +1.00 V (vs SCE) for 20 cycle scans at a scan rate of 10 mV s^{-1} in a deoxygenated solution containing 10 mmol L^{-1} BBY and a 1.00 mg mL^{-1} suspension of graphene oxide in 0.1 mol L^{-1} HCl. After coating, the platform was washed abundantly with deionized water and applied to a potential of −0.30 V (vs SCE) for 1 h in 0.50 mol L^{-1} KCl solution (pH 2.00). The two new platforms (FTO/poli(azo-BBY) and FTO/rGO) were prepared under the same conditions.

Resistance Measurements and Dissolved O_2 Detection. The electrical resistance of the platform was analyzed, using EIS measurements over an applied potential range of −0.40 V to +0.20 V (vs SCE) in a 0.05 mol L^{-1} (pH 7.4) phosphate buffer solution (PBS), by the incidence of a sinusoidal perturbation of 10 mV amplitude applied over the frequency range from 50 kHz to 0.1 Hz (10 step/dec). The saturated solutions used in the studies were obtained by bubbling with high purity O_2. All spectra were recorded at 37 °C. The analysis of the complex plane impedance spectra was determined by ZPlot 2.4 software. The determination of dissolved oxygen was performed after the addition of an aliquot of a Na_2SO_3 standard solution (0.1 mol L^{-1}). The gas concentration was calculated from the chemical reaction of oxygen consumption by sulfite. Values obtained through a commercial dissolved oxygen sensor model Hanna HI9147 were also used for comparison.

Real-Time Monitoring of Mitochondrial Oxygen Consumption. The study was approved by the Ethics Committee on Animal Use (CEUA) of UNESP—Presidente Prudente Campus, protocol no 12/2017, following the National Guidelines of the Brazilian College of Animal Experimentation and the National Guidelines for Ethical Use of Animals in Research. The animals (male Wistar rats) were divided into 4 groups: control (C), exercised (E), smoker (S), and smoker/exercised (SA) groups. All animals were subjected to 6 h fasting before euthanasia by intraperitoneal administration of sodium thiopental (60 mg/kg body weight) anesthetic after removal of the gastrocnemius skeletal muscle. The analysis of functional mitochondria was performed by saponin in muscle fibers in situ, without the isolation of organelles.[16]

The applicability of the sensor was based on protocols that evaluate the performance of mitochondrial activities.[6b,16,17] Oxygen consumption measurements were made by incubating the tissue in respiratory buffer containing 0.50 mmol L^{-1} EGTA, 3.0 mmol L^{-1} $MgCl_2$, 60 mmol L^{-1} lactobionic acid, 20 mmol L^{-1} taurine, 10 mmol

L^{-1} KH_2PO_4, 20 mmol L^{-1} HEPES, 0.11 mol L^{-1} D-sucrose, and 1 g L^{-1} BSA at 37 °C. ROUTINE (R), LEAK (L), and OXPHOS (P) respiration rates were calculated by averaging the last three measurements after achieving a steady state. ROUTINE was obtained after the addition of the tissue, LEAK after addition of 5 mmol L^{-1} pyruvate, and OXPHOS after addition of 5 mmol L^{-1} ADP and 10 mmol L^{-1} succinate. All measurements were recorded at 37 °C.

RESULTS AND DISCUSSION

Impedance Study of the Poly(azo-BBY)-rGO Nanocomposite Film. The development of the chemiresistor sensor based on poly(azo-BBY)-rGO nanocomposite was designed to include the desired properties of conductive azo-polymers and graphene. Azo-polymers exhibit high sensitivity to molecular oxygen, which selectively reacts through the diazo active sites present in its polymeric structure.[15,18] Moreover, azo-polymers exhibit extensive π-conjugation in which small perturbations at specific points of the polymer chain are reflected in the electronic properties of the material.[19] These disturbances, in the case of the poly(azo-BBY), occur through the "off" and "on" possibilities of the diazo active sites in the π-conjugated polymer chain system (Figure S1). Graphene was introduced into the material to speed the rate of the electronic response, as well as to strengthen the chemical and mechanical resistance.[20]

The electrical resistivity properties of electrodes coated with rGO, poly(azo-BBY), and poly(azo-BBY)-rGO at an applied −0.30 V (vs SCE) were investigated by electrochemical impedance spectroscopy (EIS) in 0.05 mol L^{-1} PBS (pH 7.4) in both the absence and presence of O_2, as represented in Figure 1A and B, respectively. This applied potential was chosen because it is coincident with reduction of the azo groups of the polymer by cyclic voltammogram (Figure S2). Table 1 shows the impedance parameters obtained according to the electrical circuit described for each platform (inside table). The plot of phase vs frequency was used to guide the proposal of equivalent circuit models for each studied platform (Figures 1C and D).

In general, the equivalent circuit models assigned to the platforms exhibited two constant phase elements (CPE), corresponding to the double electric (CPE_{dl}) and deposited film (CPE_{film}) layers, with one charge transfer resistance (R_{ct}). The rGO film exhibited a high value of CPE_{film} with a phase
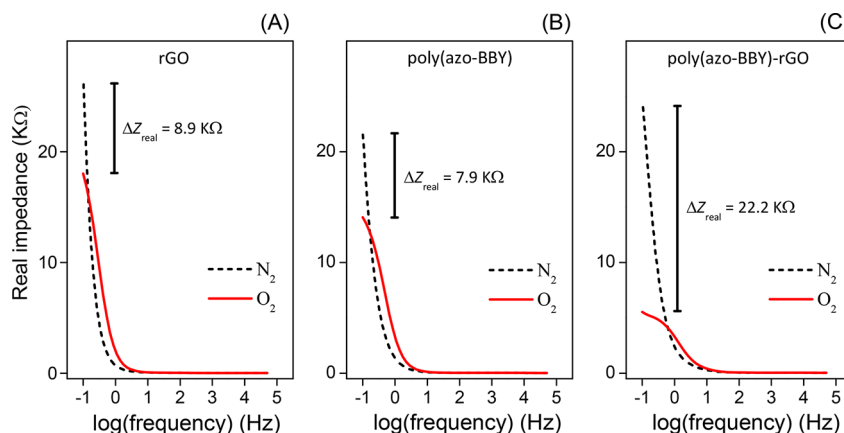
Figure 2. Real impedance response to the frequency (0.1 Hz−50 kHz) for electrodes coated with rGO (A); poly(azo-BBY) (B); poly(azo-BBY)-rGO (C) in 0.05 mol L^{-1} PBS (pH 7.4) and saturated with N$_2$ (short dash) or O$_2$ (red line). Applied potential = −0.30 V (vs SCE).

angle close to 90° (see Figure 1C), which agrees with previous studies reporting the charge storage capacity of graphene in the development of supercapacitors.[21] The poly(azo-BBY)-rGO film also displayed a high value of CPE$_{film}$, revealing that the nanocomposite film maintains the charge capacity of graphene. However, the electrode coated with poly(azo-BBY)-rGO film presented an equivalent circuit composed of two parallel R CPE combinations. The first resistance (R_{ct}) was associated with the solution/rGO interface, while the second resistance (R_{ct}*) was attributed to the rGO/poly(azo-BBY) interface. This model was confirmed by a Bode plot exhibiting two phase angle peaks (red circle—Figure 1D). The charge transfer resistance (0.08 kΩ cm^2) decreased substantially in relation to the rGO/FTO electrode (92.4 kΩ cm^2), indicating the smaller interface electron transfer resistance. This indicates the existence of the synergistic effect between graphene and poly(azo-BBY), where the space and gaps between graphene moieties were filled with polymer in the direct network formation.[22]

Comparing spectra in saturated oxygen solution, as in Figure 1B, differences are most noticeable in the radius of the semicircle arc. In all studied electrodes, the film resistance values were significantly lower than the values obtained in the absence of dissolved oxygen (Table 1). In the case of the electrode coated with poly(azo-BBY)-rGO film, the presence of oxygen in moderation led to a decrease in the impedance value, with the film resistance decreasing from 49.6 to 2.55 kΩ cm^2. This decrease clearly indicates the contribution of the reaction between polymer and oxygen.

To verify the greater sensitivity of the electrode coated with poly(azo-BBY)-rGO to that of graphene and polymer only, the real impedance variation as a function of applied frequency was studied. Figure 2 shows the real impedance values for the rGO, poly(azo-BBY), and poly(azo-BBY)-rGO films in the presence of solutions saturated with N$_2$ and O$_2$.

When compared with imaginary impedance, real impedance more directly contributed to the values associated with charge transfer resistance. The rGO, poly(azo-BBY), and poly(azo-BBY)-rGO films exhibited decreasing Z_{real} values at 0.1 Hz in the solution containing dissolved O$_2$, as observed previously. However, the greatest difference in impedance response (ΔZ_{real} = 22.2 kΩ cm^2) was attributed to the electrode coated with poly(azo-BBY)-rGO (Figure 2C). The decrease in the resistance of poly(azo-BBY)-rGO nanocomposite was approximately 60% and 64% in comparison to rGO and poly(azo-

BBY), respectively. The poly(azo-BBY)-rGO material provided real impedance change over the frequency range from 0.1 to 1 Hz. As observed, the change in real impedance is visible only at low frequencies, whereas the phase shift is more distinctive— especially in the presence of dissolved oxygen (see Figure 1D). The decrease of the real impedance is mainly due to the decreasing charge transfer resistance (R_{ct}*) of the poly(azo-BBY)-rGO as oxygen concentration increases. The R_{ct}* results from the reaction between molecular oxygen and hydrazo-benzene groups present in the polymer.[15] The reaction generates the "on" π-conjugated system in the polymer, increasing the electronic conductivity between the conjugated network of polymer and graphene.[23]

Optimization of Measurement Parameters for the Oxygen Chemiresistor Sensor. Because the impedance parameters of the poly(azo-BBY)-rGO material depend on the O$_2$ concentration of the solution, a precise determination of the applied frequency is very important in the context of possible applications for sensing small amounts of oxygen. Figure 3A shows the real impedance response of the sensor as a function of the dissolved oxygen concentration (0.17−1.03 mmol L^{-1}). The maximum changes in the impedance are observed at frequencies of less than 0.5 Hz, which is the region that most reflects the charge resistance. It is evident that the resistance tended to reach a minimum when O$_2$ concentration in the solution reached saturation. We have previously seen that the impedance of the poly(azo-BBY)-rGO is dependent on the applied frequency range. As illustrated in Figure 3B, the response range of the sensor decreased gradually with increasing applied frequency. The sensitivity of the sensor (see Figure 3C) extracted from the calibration curve was also dependent on applied frequency. The applied frequency of 0.1 Hz was chosen as a better operational parameter for the next study step.

The use of the chrono-impedance technique for real time monitoring of dissolved oxygen variation in phosphate buffer (pH 7.4) was evaluated. The chrono-impedance response to small variations of oxygen concentration was achieved by first saturating the electrolyte solution with O$_2$, then consuming small amounts of O$_2$ by injecting aliquots of sulfite. A typical response of the sensor, recorded at different O$_2$ concentrations, is shown in Figure 4A. The appreciable change in the impedance response reflects the possibility of sensor application in monitoring mitochondrial oxygen consumption.

(A)

(B)

(C)
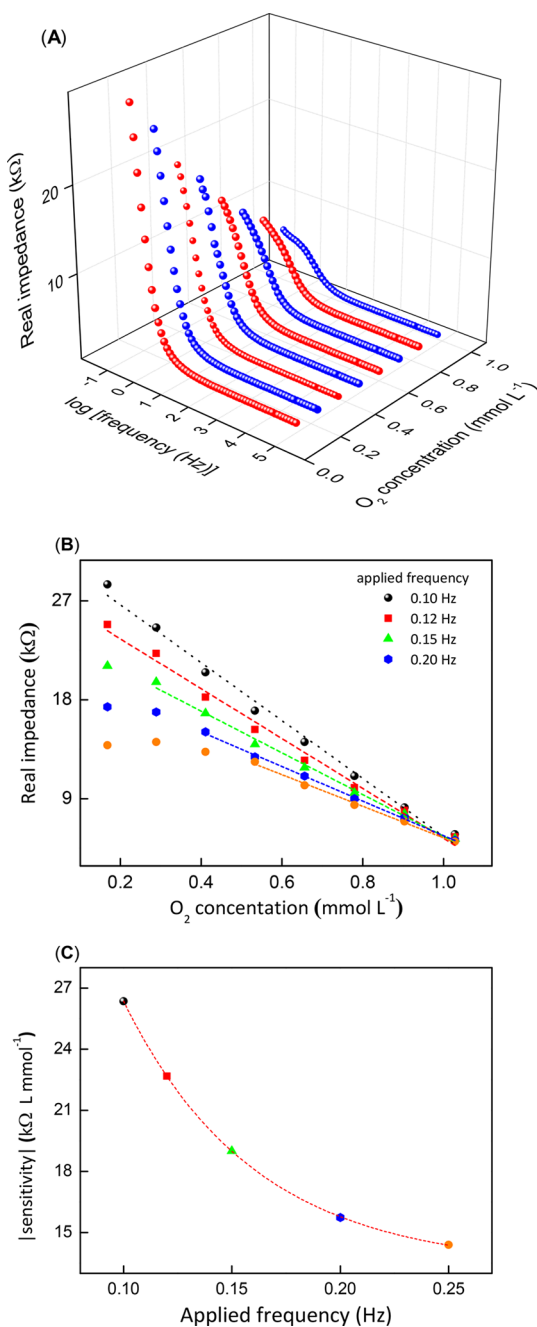
Figure 3. (A) 3D Bode impedance magnitude plot recorded for the chemiresistor sensor as a function of the applied frequency at different concentrations of dissolved oxygen in the range of 0.13−1.03 mg L^{-1} in 0.05 mol L^{-1} PBS (pH 7.4). Applied potential = −0.30 V vs SCE. (B) Sensor response versus O$_2$ concentration at applied frequencies ranging 0.10 to 0.25 Hz. (C) Sensitivity of the oxygen sensor versus applied frequency. The sensitivity was extracted from Figure 3B.
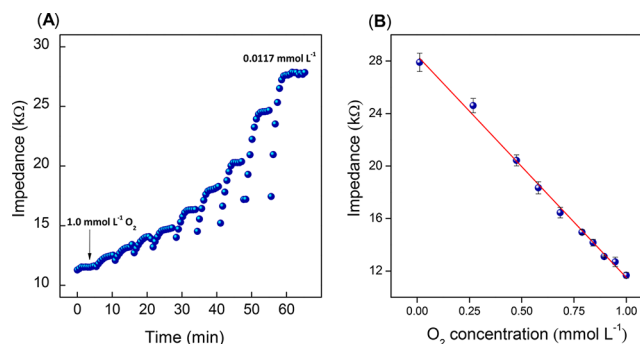
Figure 4B shows a linear relationship between the impedance magnitude and dissolved oxygen concentration in the range of 0.0117 mmol L^{-1} to 1.02 mmol L^{-1}:

$$\text{Impedence (k}\Omega) = (28.4 \pm 0.3) - (16.8 \pm 0.4)[O_2] \ (\text{mmol L}^{-1})$$

$$(n = 10; \ r = 0.9976)$$

with a detection limit of 0.360 μmol L^{-1}.

The dynamic impedance response of the poly(azo-BBY)-rGO sensor (Figure S3) was examined in PBS solutions,


(A)

(B)

Figure 4. (A) Chrono-impedance response of the chemiresistor sensor at different dissolved oxygen concentrations in 0.05 mol L^{-1} PBS (pH 7.4). Applied frequency = 0.10 Hz. Applied potential = −0.30 V (vs SCE). (B) Calibration curve for the chemiresistor sensor as a function of dissolved oxygen concentration. The error bars represent the standard deviation from three separate experiments using the same sensor.

saturated with O$_2$ and N$_2$, with an applied frequency of 0.1 Hz. The sensor exhibited good reversibility and reproducibility with a relative variation of 4.1% in the overall response of the chemiresistor per regeneration cycle. The response time to dissolved oxygen was quite rapid, with an apparent response time of ±3 min. This time meets expectations for the applied purpose of the chemiresistor sensor in biological systems, since similar measurements require several minutes to stabilize after each mitochondrial stimulus-response.[16]

Chemiresistor Sensor Applications in Real-Time Monitoring of Mitochondrial Oxygen. To address the application of the sensor on mitochondrial respiration, mitochondrial O$_2$ consumption corresponding to the response of each electron transport chain complex was measured during a sequential substrate addition protocol.[16,24] The competition for these substrates (pyruvate, ADP, succinate, and cytochrome c) was ascertained by the direct response of sensor as shown by chrono-impedance measurements of the dissolved O$_2$ (1.00 mmol L^{-1}). Figure S4 shows the interference study in the impedance response of the sensor. The analyzed substrates were not considered to interfere when the relative response in the measured impedance was less than 5%.

The performance of the sensor in real-time monitoring of mitochondrial oxygen consumption was assessed in tissue samples collected from the skeletal muscle from 4 different groups of rats: control (C), smokers (F), smokers exercised (FE), and exercised (E). Mitochondrial respiration can be evaluated, in general, according to the respiration type. There are three main types of respiration:[24,25] (1) the ROUTINE (R) respiration state is the demand for cellular oxygen at steady-state without any additions to the cell medium; (2) the LEAK (L) respiration state is an acronym for the resting oxygen flux compensating for proton leak, proton slip, and cation cycling and is related to the generation of reactive oxidative species (ROS); (3) the OXPHOS (P) respiration state is the mitochondrial respiratory capacity to produce ATP. Figure 5 illustrates real-time measurements of cellular oxygen consumption by studied tissue in respiratory buffer using the proposed sensor. The decrease in the oxygen concentration (red line) was detected by the sensor for each injection of tissue (R) and pyruvate (L). The addition of ADP (P) and succinate (P) substantially increased oxygen consumption by activating mitochondrial oxidative phosphorylation. This
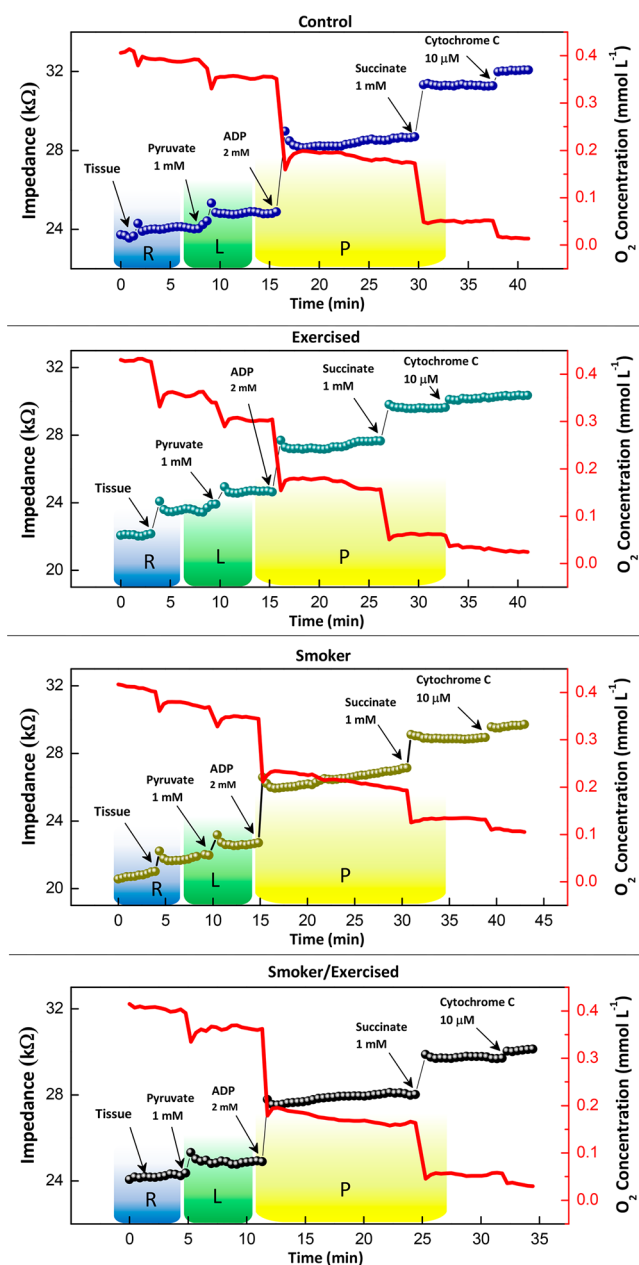
Figure 5. Representative trace respiration titration protocol measuring oxygen concentrations (red line, right y-axis) over time (minutes). O_2 concentration was calculated from the calibration curve using the values of $[O_2]_{max}$ and $[O_2]_{zero}$. Titrations of mitochondrial substrates and their time of addition are shown with arrows. Respiration states are indicated by color backgrounds: (R) routine = blue; (L) leak = green; and (P) oxphos = yellow. $t = 37\ °C$.

Table 2. Mitochondrial Oxygen Consumption[a]

	Oxygen respiration flux ($\mu mol\ g^{-1}\ L^{-1}\ s^{-1}$)		
Test group	ROUTINE	LEAK	OXPHOS
Control	17.2 ± 2.1	25.4 ± 1.0	132.2 ± 3.9
Exercised	74.2 ± 5.7	25.7 ± 2.1	165.3 ± 4.1
Smoker	10.0 ± 2.3	28.3 ± 1.9	143.0 ± 4.4
Smoker/Exercised	19.3 ± 3.1	27.8 ± 1.8	104.0 ± 6.2

[a]The rate of oxygen consumption in different states of mitochondrial respiration. Values represent the mean for a set of three animals.

substrates confirms the maintenance of an intact and functional respiratory chain when tissues are suspended in the respiratory buffer.

CONCLUSION

The chemiresistor platform based on the poly(azo-BBY)-rGO nanocomposite film was demonstrated to be a simple, sensitive, and selective sensor for O_2 detection in mitochondrial respiration. The application of the proposed sensor for the real-time monitoring of mitochondrial oxygen consumption during a sequential substrate addition protocol was consistent with similar techniques in the biological area.

ASSOCIATED CONTENT

ⓢ Supporting Information

The Supporting Information is available free of charge on the ACS Publications website at DOI: 10.1021/acssensors.8b01013.

Schematic representation of the conducting azo-polymer; electrochemical response of the azo-polymer; transient responses of the oxygen sensor and the selectivity of the sensor (PDF)

AUTHOR INFORMATION

Corresponding Author

*E-mail: marcos.fs.teixeira@unesp.br. Tel.: +55 18 3229 57 49. Fax: + 55 18 3221 56 82.

ORCID ⓘ

Marcos F. S. Teixeira: 0000-0001-9355-2143

Notes

The authors declare no competing financial interest.

ACKNOWLEDGMENTS

REFERENCES

(1) Scheffler, I. E. *Mitochondria*, 2nd ed.; Wiley-Liss: Hoboken, NJ, 2008.

(2) Scheffler, I. E. Mitochondrial Electron Transfer and Oxidative Phosphorylation. *Mitochondria* **2007**, 168−297.

(3) (a) Spinazzi, M.; Casarin, A.; Pertegato, V.; Ermani, M.; Salviati, L.; Angelini, C. Optimization of respiratory chain enzymatic assays in muscle for the diagnosis of mitochondrial disorders. *Mitochondrion* **2011**, *11* (6), 893−904. (b) Lebiedzinska, M.; Karkucinska-Wieckowska, A.; Giorgi, C.; Karczmarewicz, E.; Pronicka, E.; Pinton, P.; Duszynski, J.; Pronicki, M.; Wieckowski, M. R. Oxidative stress-dependent p66Shc phosphorylation in skin fibroblasts of children with mitochondrial disorders. *Biochim. Biophys. Acta, Bioenerg.* **2010**, *1797* (6−7), 952−960. (c) Gnaiger, E.;

indicated that respiration was substrate dependent. Cytochrome c was added at the end of the measurements to verify mitochondrial integrity, and no significant effect was detected across all samples. The oxygen consumption rates (Table 2) were calculated for each substrate injected into the system in the four test groups, according to the literature descriptions.[6b,26]

The evaluation of the functional performance of mitochondria is not the main focus of this manuscript, but the results obtained may indicate applicability of the proposed sensor. These results clearly show the ability of the proposed sensor to monitor the oxygen consumption with respiratory chain

SteinlechnerMaran, R.; Mendez, G.; Eberl, T.; Margreiter, R. Control of mitochondrial and cellular respiration by oxygen. *J. Bioenerg. Biomembr.* **1995**, *27* (6), 583−596. (d) Lin, M. T.; Beal, M. F. Mitochondrial dysfunction and oxidative stress in neurodegenerative diseases. *Nature* **2006**, *443* (7113), 787−795.

(4) (a) van der Windt, G. J. W.; Everts, B.; Chang, C. H.; Curtis, J. D.; Freitas, T. C.; Amiel, E.; Pearce, E. J.; Pearce, E. L. Mitochondrial Respiratory Capacity Is a Critical Regulator of CD8(+) T Cell Memory Development. *Immunity* **2012**, *36* (1), 68−78. (b) Alston, C. L.; Rocha, M. C.; Lax, N. Z.; Turnbull, D. M.; Taylor, R. W. The genetics and pathology of mitochondrial disease. *J. Pathol* **2017**, *241* (2), 236−250. (c) Yao, J.; Irwin, R. W.; Zhao, L. Q.; Nilsen, J.; Hamilton, R. T.; Brinton, R. D. Mitochondrial bioenergetic deficit precedes Alzheimer's pathology in female mouse model of Alzheimer's disease. *Proc. Natl. Acad. Sci. U. S. A.* **2009**, *106* (34), 14670−14675.

(5) (a) Nogawa, M.; Ching, C. T.; Ida, T.; Itakura, K.; Takatani, S. A new hybrid reflectance optical pulse oximetry sensor mor lower oxygen saturation measurement and for broader clinical application. *Proc. SPIE* **1997**, *2976*, 78−87. (b) Kaur, A.; Jankowska, K.; Pilgrim, C.; Fraser, S. T.; New, E. J. Studies of Hematopoietic Cell Differentiation with a Ratiometric and Reversible Sensor of Mitochondrial Reactive Oxygen Species. *Antioxid. Redox Signaling* **2016**, *24* (13), 667−679. (c) Liu, H. W.; Xu, S.; Wang, P.; Hu, X. X.; Zhang, J.; Yuan, L.; Zhang, X. B.; Tan, W. H. An efficient two-photon fluorescent probe for monitoring mitochondrial singlet oxygen in tissues during photodynamic therapy. *Chem. Commun.* **2016**, *52* (83), 12330−12333. (d) Zhang, X.; Gao, F. Imaging mitochondrial reactive oxygen species with fluorescent probes: Current applications and challenges. *Free Radical Res.* **2015**, *49* (4), 374−382. (e) Dickinson, B. C.; Srikun, D.; Chang, C. J. Mitochondrial-targeted fluorescent probes for reactive oxygen species. *Curr. Opin. Chem. Biol.* **2010**, *14* (1), 50−56. (f) Villamena, F. A., Electrochemical, Mass Spectroscopic, Immunochemical, and Nuclear Magnetic Resonance Techniques. In *Reactive Species Detection in Biology: From Fluorescence to Electron Paramagnetic Resonance Spectroscopy*, 2017, pp 253−322. (g) Aragones, J.; Fraisl, P.; Baes, M.; Carmeliet, P. Oxygen Sensors at the Crossroad of Metabolism. *Cell Metab.* **2009**, *9* (1), 11−22.

(6) (a) Paital, B.; Samanta, L. A Comparative Study of Hepatic Mitochondrial Oxygen Consumption in Four Vertebrates by Using Clark-Type Electrode. *Acta Biol. Hung.* **2013**, *64* (2), 152−160. (b) Li, Z. H.; Graham, B. H. Measurement of Mitochondrial Oxygen Consumption Using a Clark Electrode. *Methods Mol. Biol.* **2012**, *837*, 63−72. (c) Silva, A. M.; Oliveira, P. J. Evaluation of Respiration with Clark Type Electrode in Isolated Mitochondria and Permeabilized Animal Cells. *Methods Mol. Biol.* **2012**, *810*, 7−24. (d) Simonnet, H.; Vigneron, A.; Pouyssegur, J. Conventional Techniques to Monitor Mitochondrial Oxygen Consumption. *Methods Enzymol.* **2014**, *542*, 151−161.

(7) (a) Liana, D. D.; Raguse, B.; Wieczorek, L.; Baxter, G. R.; Chuah, K.; Gooding, J. J.; Chow, E. Sintered gold nanoparticles as an electrode material for paper-based electrochemical sensors. *RSC Adv.* **2013**, *3* (23), 8683−8691. (b) Lange, U.; Mirsky, V. M. Chemiresistors based on conducting polymers: A review on measurement techniques. *Anal. Chim. Acta* **2011**, *687* (2), 105−113.

(8) (a) Wordofa, D. N.; Ramnani, P.; Tran, T. T.; Mulchandani, A. An oligonucleotide-functionalized carbon nanotube chemiresistor for sensitive detection of mercury in saliva. *Analyst* **2016**, *141* (9), 2756−2760. (b) Myers, M.; Cooper, J.; Pejcic, B.; Baker, M.; Raguse, B.; Wieczorek, L. Functionalized graphene as an aqueous phase chemiresistor sensing material. *Sens. Actuators, B* **2011**, *155* (1), 154−158. (c) Webster, M. S.; Cooper, J. S.; Chow, E.; Hubble, L. J.; Sosa-Pintos, A.; Wieczorek, L.; Raguse, B. Detection of bacterial metabolites for the discrimination of bacteria utilizing gold nanoparticle chemiresistor sensors. *Sens. Actuators, B* **2015**, *220*, 895−902. (d) Hangarter, C. M.; Chartuprayoon, N.; Hernandez, S. C.; Choa, Y.; Myung, N. V. Hybridized conducting polymer chemiresistive nano-sensors. *Nano Today* **2013**, *8* (1), 39−55.

(9) (a) Koudehi, M. F.; Pourmortazavi, S. M. Polyvinyl Alcohol/ Polypyrrole/Molecularly Imprinted Polymer Nanocomposite as Highly Selective Chemiresistor Sensor for 2,4-DNT Vapor Recognition. *Electroanalysis* **2018**, *30* (10), 2302−2310. (b) Alizadeh, T.; Rezaloo, F. Toluene chemiresistor sensor based on nano-porous toluene-imprinted polymer. *Int. J. Environ. Anal. Chem.* **2013**, *93* (8), 919−934.

(10) Kim, D. H.; Jang, J. S.; Koo, W. T.; Choi, S. J.; Cho, H. J.; Kim, M. H.; Kim, S. J.; Kim, I. D. Bioinspired Cocatalysts Decorated WO3 Nanotube Toward Unparalleled Hydrogen Sulfide Chemiresistor. *Acs Sensors* **2018**, *3* (6), 1164−1173.

(11) Wang, K.; Yang, H.; Qian, X. M.; Xue, Z.; Li, Y. J.; Liu, H. B.; Li, Y. L. Inorganic/organic small molecular semiconductor self-assembly to functional core-shell nanoarchitectures for ultrasensitive chemiresistors to aniline vapor. *Dalton T* **2014**, *43* (30), 11542−11547.

(12) Ogata, A. F.; Song, S. W.; Cho, S. H.; Koo, W. T.; Jang, J. S.; Jeong, Y. J.; Kim, M. H.; Cheong, J. Y.; Penner, R. M.; Kim, I. D. An Impedance-Transduced Chemiresistor with a Porous Carbon Channel for Rapid, Nonenzymatic, Glucose Sensing. *Anal. Chem.* **2018**, *90* (15), 9338−9346.

(13) Basnayaka, P. A.; Ram, M. K.; Stefanakos, L.; Kumar, A. High performance graphene-poly (o-anisidine) nanocomposite for supercapacitor applications. *Mater. Chem. Phys.* **2013**, *141* (1), 263−271.

(14) (a) Gupta, S.; Price, C. Investigating graphene/conducting polymer hybrid layered composites as pseudocapacitors: Interplay of heterogeneous electron transfer, electric double layers and mechanical stability. *Composites, Part B* **2016**, *105*, 46−59. (b) Gupta, S.; Heintzman, E.; Price, C. Electrostatic Layer-By-Layer Self-Assembled Graphene/Multi-Walled Carbon Nanotubes Hybrid Multilayers as Efficient 'All Carbon' Supercapacitors. *J. Nanosci. Nanotechnol.* **2016**, *16* (5), 4771−4782. (c) Gupta, S.; McDonald, B.; Carrizosa, S. B.; Price, C. Microstructure, residual stress, and intermolecular force distribution maps of graphene/polymer hybrid composites: Nanoscale morphology-promoted synergistic effects. *Composites, Part B* **2016**, *92*, 175−192.

(15) Teixeira, M. F. S.; Barsan, M. M.; Brett, C. M. A. Molecular engineering of a pi-conjugated polymer film of the azo dye Bismarck Brown Y. *RSC Adv.* **2016**, *6* (103), 101318−101322.

(16) Kuznetsov, A. V.; Veksler, V.; Gellerich, F. N.; Saks, V.; Margreiter, R.; Kunz, W. S. Analysis of mitochondrial function in situ in permeabilized muscle fibers, tissues and cells. *Nat. Protoc.* **2008**, *3* (6), 965−976.

(17) Gnaiger, E. High-resolution respirometry for the study of mitochondrial function in health and disease. The OROBOROS Oxygraph-2k. *Shock* **2005**, *23*, 6.

(18) Li, X. G.; Huang, M. R.; Duan, W.; Yang, Y. L. Novel multifunctional polymers from aromatic diamines by oxidative polymerizations. *Chem. Rev.* **2002**, *102* (9), 2925−3030.

(19) Wang, X. Azo Polymers: Synthesis, Functions and Applications. *Soft Biol. Matter* **2017**, 1−230.

(20) Salavagione, H. J.; Martinez, G.; Ellis, G. Recent Advances in the Covalent Modification of Graphene With Polymers. *Macromol. Rapid Commun.* **2011**, *32* (22), 1771−1789.

(21) (a) Ambrosi, A.; Pumera, M. Electrochemically Exfoliated Graphene and Graphene Oxide for Energy Storage and Electrochemistry Applications. *Chem. - Eur. J.* **2016**, *22* (1), 153−159. (b) Shao, Y. L.; El-Kady, M. F.; Wang, L. J.; Zhang, Q. H.; Li, Y. G.; Wang, H. Z.; Mousavi, M. F.; Kaner, R. B. Graphene-based materials for flexible supercapacitors. *Chem. Soc. Rev.* **2015**, *44* (11), 3639−3665. (c) Shao, Y. L.; El-Kady, M. F.; Lin, C. W.; Zhu, G. Z.; Marsh, K. L.; Hwang, J. Y.; Zhang, Q. H.; Li, Y. G.; Wang, H. Z.; Kaner, R. B. 3D Freeze-Casting of Cellular Graphene Films for Ultrahigh-Power-Density Supercapacitors. *Adv. Mater.* **2016**, *28* (31), 6719.

(22) Hu, K. S.; Kulkarni, D. D.; Choi, I.; Tsukruk, V. V. Graphene-polymer nanocomposites for structural and functional applications. *Prog. Polym. Sci.* **2014**, *39* (11), 1934−1972.

(23) Inzelt, G. R. *Conducting polymers: a new era in electrochemistry*, 2nd ed.; Springer: Heidelberg; New York, 2012.

(24) Makrecka-Kuka, M.; Krumschnabel, G.; Gnaiger, E. High-Resolution Respirometry for Simultaneous Measurement of Oxygen and Hydrogen Peroxide Fluxes in Permeabilized Cells, Tissue Homogenate and Isolated Mitochondria. *Biomolecules* **2015**, *5* (3), 1319−1338.

(25) Lemieux, H.; Blier, P. U.; Gnaiger, E. Remodeling pathway control of mitochondrial respiratory capacity by temperature in mouse heart: electron flow through the Q-junction in permeabilized fibers. *Sci. Rep.* **2017**, *7*, 1 DOI: 10.1038/s41598-017-02789-8.

(26) Kueh, H. Y.; Niethammer, P.; Mitchison, T. J. Maintenance of Mitochondrial Oxygen Homeostasis by Cosubstrate Compensation. *Biophys. J.* **2013**, *104* (6), 1338−1348.